

Low-Complexity Subband Equalization of Mobile Underwater Acoustic Channels

Konstantinos Pelekanakis and Mandar Chitre

Acoustic Research Laboratory, National University of Singapore, Singapore, 119223

E-mail: {costas, mandar}@arl.nus.edu.sg

Abstract—The intersymbol interference (ISI) caused by multipath propagation becomes the major challenge for designing efficient equalization methods for underwater acoustic communications. Even at moderate bit-rates, the computational complexity of adaptive equalizers is high enough to challenge their real-time implementation. Hence, reducing their complexity by either low-complexity algorithms or efficient receiver structures is of paramount importance. In this work, we revisit the idea of joint subband equalization [9] and propose new receivers with reduced computational complexity that can cope with variable platform mobility within a signal packet, track rapid multipath fluctuations and maintain robustness under impulsive noise environments. The proposed subband equalizers are successfully tested in two experimental shallow water links by detecting quadrature phase-shift keying (QPSK) signals. In addition, results based on their performance-complexity tradeoffs are reported.

I. INTRODUCTION

The achievable data rate of underwater acoustic communication systems over horizontal links is severely affected by signal distortions due to long multipath propagation. Especially for single-carrier phase-coherent systems, mitigating the intersymbol interference (ISI) caused by multipath, is the major challenge of a system designer. Optimal ISI-compensation techniques, such as maximum likelihood sequence detection, are computational intensive and often not practical in most real-life applications. A sub-optimal, but, practical approach is a receiver that uses an adaptive equalizer [1],[2] or a multi-sensor adaptive equalizer with spatial diversity combining [3]. These types of receivers have been successfully tested in various shallow and deep water seas and have become the underlying technology of commercially available acoustic modems. Reducing the computational complexity of these systems is an active research topic because the spatiotemporal filters that typically operate on the received data require about a hundred of coefficients even at few kilobits per second (kbps).

The task of reducing computational complexity can be tackled either by designing more efficient signal processing algorithms or more efficient receiver structures or a combination of both. Linear complexity adaptive algorithms, such as the least mean squares (LMS) [4], are typically preferred for chip implementation. Motivated by this fact, the authors recently introduced algorithmic frameworks for designing linear complexity channel estimation algorithms that exploit the sparse multipath profile [5],[6]. An example of a low-complexity equalizer structure has been presented in [7]. This structure

manages to significantly reduce the number of channels in a multi-sensor equalizer by employing a spatial pre-combiner in the front-end of the receiver. An extension of the work in [7] has been proposed in [8], where a pre-combiner was coupled with a linear complexity sparse channel estimation algorithm. Channel sparseness was exploited to determine the significant coefficients of the adaptive equalizer, thus reducing its size.

Since the number of receiver parameters grows linearly with the signal bandwidth, a direct way to reduce complexity in single-input single-output systems is to split the bandwidth into contiguous subbands and transmit the same data across different subbands [9]. Treating each subband as a separate "channel" and using a multichannel equalizer, explicit frequency diversity is exploited, and thus, link reliability is improved. A notable characteristic of this system is that it can compensate only for constant transmitter/receiver motion, which may not be adequate if there is accelerating motion during reception of the transmitted signal.

Another motivation for subband processing is based on the fact that higher subbands are expected to have more sparse multipath arrivals as well as shorter multipath spreads than lower subbands. This can be explained due to frequency dependent absorption: higher frequencies undergo higher attenuation. Consequently, employing different channel estimation algorithms for different subbands is appealing because the *performance-complexity tradeoff* can be addressed more efficiently. In addition, when the ambient noise is impulsive, such as ice cracking [10] and snapping shrimp noise [11], [12], subband signal processing limits the distorting effect of the impulse.

Capitalizing on the improved-proportionate M-estimate affine projection algorithm (IPMAPA) [6], novel channel-estimate-based decision feedback equalizer (DFE) structures of different complexities are proposed. These receivers cope with time-varying motion during transmission, exploit different sparse multipath profiles of different subbands and achieve robustness under impulsive noise. Two links from a recent underwater experiment in Singapore Sea are used to compare the proposed receivers in terms of their symbol-error-rates (SERs) as a function of the received signal-to-noise ratio (SNR).

Notation: Superscripts $(\cdot)^T$, $(\cdot)^\dagger$, and $(\cdot)^*$ stand for transpose, Hermitian transpose, and conjugate, respectively. Column vectors (matrices) are denoted by boldface lowercase (uppercase) letters. Let $z \in \mathbb{C}$ and $p \geq 1$. The L_p norm of z

is defined as $|z|_p \triangleq (|\operatorname{Re}\{z\}|^p + |\operatorname{Im}\{z\}|^p)^{1/p}$. Let $\mathbf{z} \in \mathbb{C}^N$. The L_p norm of \mathbf{z} is defined as $\|\mathbf{z}\|_p \triangleq (\sum_{i=0}^{N-1} |z_i|_p^p)^{1/p}$.

II. SYSTEM MODEL AND ARCHITECTURE

A. Transmitter architecture

The transmit system is shown in Fig. 1(a). The information-bearing symbol stream $\{d_n\}$ is generated from linear and memoryless modulation methods such as phase-shift keying (PSK). $\{d_n\}$ is pulse shaped and modulated into subband m . The raised cosine (RC) filter with signaling interval T and roll-off factor α is used for pulse shaping. The transmitted waveform $x(t)$ is given by

$$u(t) = \sum_n d_n g(t - nT) \quad (1)$$

$$x(t) = \operatorname{Re} \left\{ \sum_{m=1}^M u(t) e^{j2\pi f_m t} \right\}, \quad (2)$$

where $g(t)$ is the RC impulse response and f_m denotes the center frequency of the m^{th} subband. Moreover, the m^{th} subband occupies the frequency range $f_m \pm (1+\alpha)/(2T)$ and the total operational bandwidth is the sum of the corresponding subbands with no guard bands in between. Note that the fast spectral roll-off of the RC filter renders inter-subband interference negligible for typical autonomous platform velocities.

B. Channel model

Each received subband signal is shifted to baseband, low-pass filtered and coarsely synchronized with a known chirp signal. With respect to the center frequency f_m , the baseband equivalent output $r_m(t)$ is related to the input $u(t)$ via the formula [2]

$$y_m(t) = \int_{-\infty}^{+\infty} h_m^*(\tau, t) u(t - \tau) d\tau + w_m(t), \quad (3)$$

where $h_m(\tau, t)$ and $w_m(t)$ denote, respectively, the input delay-spread function and the ambient impulsive noise. Let us assume that there is non-constant motion either by the source or the receiver platform. Since each subband signal is considered to be wideband, the received signal is time-scaled and carrier-phase-shifted as follows

$$r_m(t) = y_m(t + \Delta_m t - \tau_m) e^{j2\pi f_m (\Delta_m t - \tau_m)} + w_m(t). \quad (4)$$

Δ_m stands for the (time-varying) expansion or compression factor between the transmit and receive signal and τ_m is the arrival time of the beginning edge of the signal.

C. Receiver architecture

As our goal is to achieve high-rate communications, the symbol interval T is designed to be smaller than the multipath spread of the channel and so inter-symbol interference (ISI) is expected to occur in each subband. Considering each subband as a distinct "channel", a multi-channel DFE is proposed in Fig. 1(b). To recover the transmitted symbol d_n , there are three processing stages: adaptive resampling, robust channel estimation and decision feedback equalization.

1) *Adaptive resampling*: Let us assume that $r_m(t)$ is sampled at four samples/symbol, i.e., $r_m(n') \triangleq r_m(n'T/4)$. To compensate for the wideband distortion due to platform motion, $r_m(n')$ is resampled to 2 samples/symbol with the aid of a linear interpolator. The novelty here with respect to [13] is that adaptive resampling is coupled with channel estimation as indicated below. The output of the linear interpolator, $y_m(n)$, is given by

$$y_m(n) = (I_{n,m} r_m(n') + (I_{n,m} - 1) r_m(n'+1)) e^{-j\phi_{n,m}} \quad (5)$$

$$\phi_{n,m} = \phi_{n-1,m} + 2\pi(I_{n,m} - 1)f_m T/2 \quad (6)$$

$$I_{n,m} = I_{n-1,m} + K_p \theta_{n-1,m} \quad (7)$$

$$\theta_{n,m} = \operatorname{Im} \left\{ p_{n-1,m} \tilde{d}_{n-1}^* \right\} \quad (8)$$

where $n' = \{1, 3, 5, \dots\}$, $n = \{1, 2, \dots\}$, $\phi_{n,m}$ is the carrier-phase estimate, $I_{n,m}$ is the one-tap linear interpolator, \tilde{d}_n denotes the decision of d_n when the DFE operates in decision-directed mode or the correct symbol in training mode, $p_{n,m}$ is the output of the m^{th} feedforward equalizer during the n^{th} symbol interval and K_p is a phase tracking parameter. The parameters $\phi_{n,m}$ and $I_{n,m}$ are updated at the symbol rate with initial values $\phi_{0,m} = 0$ and $I_{0,m} = 1$.

It is worth noting that the linear interpolator compensates for the mean Doppler of the received signal, yet, there might be significant residual Doppler spread because of strong time-varying multipath. This may be experienced, for example, in horizontal links with small range-to-depth ratios. Hence, successful receiver performance depends on the ability of the adaptive equalizer to tolerate any residual Doppler spread.

2) *Robust channel estimation*: After compensating for the mean Doppler distortion, the received signal in (3) sampled at time instant nT is expressed as

$$y_m(n) = \mathbf{h}_m(n)^\dagger \mathbf{u}(n) + w_m(n), \quad (9)$$

where

$$\mathbf{u}(n) = \begin{bmatrix} u(nT - (N_c + 1)T/2) \\ \vdots \\ u(nT) \\ \vdots \\ u(nT + N_a T/2) \end{bmatrix} \quad (10)$$

and

$$\mathbf{h}_m(n) = \begin{bmatrix} h_m(nT, (N_c - 1)T/2) \\ \vdots \\ h_m(nT, 0) \\ \vdots \\ h_m(nT, -N_a T/2) \end{bmatrix} \quad (11)$$

are the samples of the input signal and the m^{th} baseband impulse response (including transmit and receive filters), respectively. The parameters N_c and N_a denote, respectively, the causal and acausal taps (coefficients) of the channel impulse response with respect to the arrival $h_m(nT, 0)$. Notice that N_c and N_a may get smaller values for higher subbands due

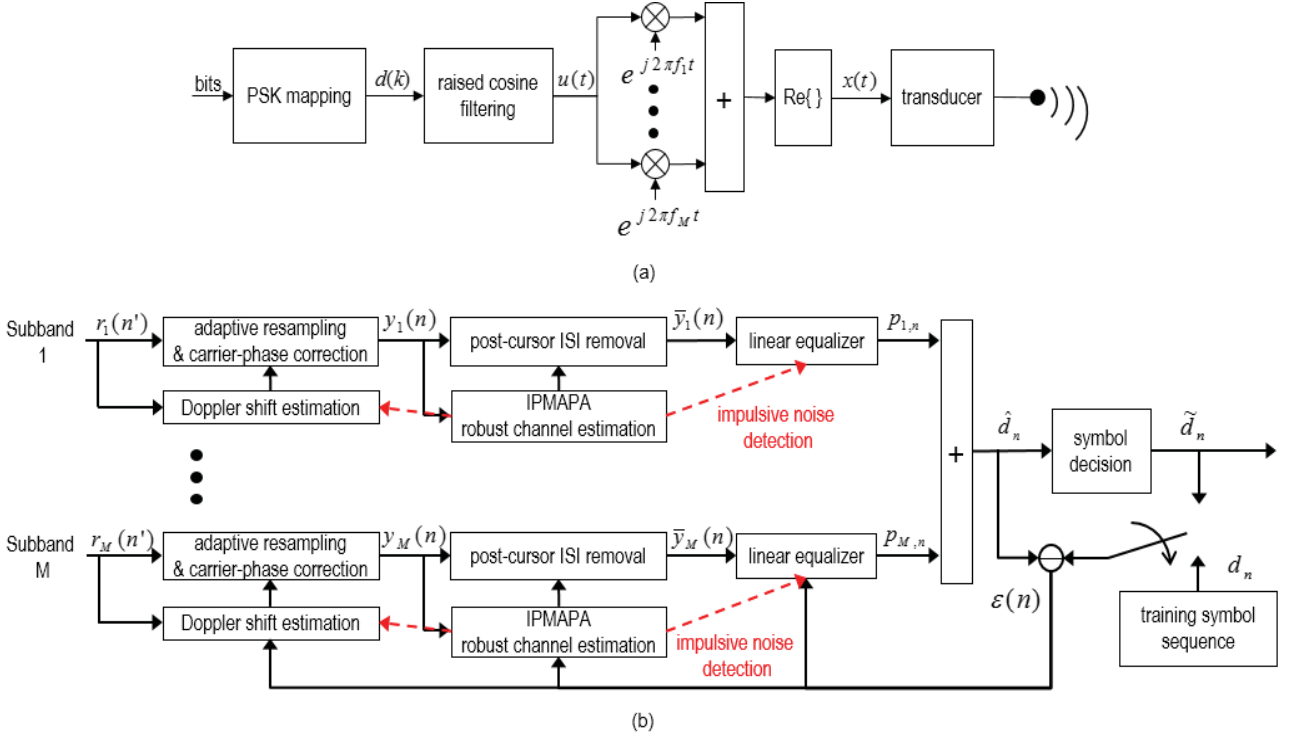


Fig. 1. (a) Block diagram of transmitter. (b) Block diagram of the subband equalizer receiver.

to frequency-dependent absorption of acoustic energy, thus reducing receiver complexity.

In impulsive noise environments, it is widely known that L_2 norm-based algorithms suffer severe performance degradation. Recently, the authors have introduced the improved-proportionate M-estimate affine projection algorithm (IPMAPA) [6], a linear complexity algorithm that exploits sparse multipath profiles while being robust against impulsive interference. Let $\hat{\mathbf{h}}$ be the channel estimate of \mathbf{h} , the IPMAPA channel update equations are (subscript m is dropped for simplicity):

$$\hat{\mathbf{h}}(n) = \hat{\mathbf{h}}(n-1) + \mu \mathbf{A}(n) \mathbf{B}(n) \mathbf{e}(n)^*, \quad (12)$$

$$\mathbf{e}(n)^* = \tilde{\mathbf{y}}(n)^* - \mathbf{U}(n)^\dagger \hat{\mathbf{h}}(n-1), \quad (13)$$

$$\tilde{\mathbf{y}}(n) = \begin{bmatrix} y_m(nT) \\ \vdots \\ y_m((n-L+1)T) \end{bmatrix} \quad (14)$$

$$\mathbf{A}(n) = \mathbf{G}(n-1) \mathbf{U}(n), \quad (15)$$

$$\mathbf{B}(n) = (\mathbf{U}(n)^\dagger \mathbf{A}(n) + \delta \mathbf{Q}(n)^{-1})^{-1}, \quad (16)$$

$$\delta = \frac{(1-\beta)\delta'}{2(N_c + N_a)}, \quad (17)$$

where L (typically $L < 5$) is a parameter that improves convergence for correlated inputs, $\mu \in (0, 1]$ is a fixed step-size parameter that dictates overall convergence, $\mathbf{U}(n) = [\mathbf{u}(n) \mathbf{u}(n-1) \dots \mathbf{u}(n-L+1)]$ is the $(N_c + N_a) \times L$ matrix of input samples, $\mathbf{G}(n)$ is a diagonal matrix with elements

$\{g(\hat{h}_i(n))\}_{i=0}^{N_c+N_a-1}$ (promotes sparse solutions), $\beta \in [-1, 1]$ is a sparseness parameter, $\mathbf{e}(n)$ stands for the $L \times 1$ prior error signal, $\mathbf{Q}(n)$ is a diagonal matrix with elements $\{q(e(n-i))\}_{i=0}^{L-1}$ (promotes robustness under impulsive noise) and $\delta' = 10P_s$ (P_s being the transmitted signal power) is a regularization parameter. Initialization of the algorithm starts with $\hat{\mathbf{h}}(0) = \mathbf{0}$. Note that the channel update equations require $O(N_c + N_a)$ computational complexity because $\mathbf{G}(n)$ is diagonal and $N_c + N_a \gg L$ for typical underwater acoustic channels. We now explain the role of the matrices \mathbf{G} and \mathbf{Q} .

a) The \mathbf{G} matrix: The purpose of the \mathbf{G} matrix is to assign a variable step size parameter to each filter tap [14]. This parameter is a function of the tap's previously estimated magnitude. As a result, active filter taps (i.e., taps with significant values) converge fast, which makes the overall algorithm to have fast convergence in sparse channels. We stress that no prior knowledge of the significant tap position is required. The diagonal elements $\{g(\hat{h}_i(n))\}_{i=0}^{N_c+N_a-1}$ of $\mathbf{G}(n)$ are given by

$$g(\hat{h}_i(n)) = \frac{1-\beta}{2(N_c + N_a)} + \frac{(1+\beta) \left| \hat{h}_i(n) \right|_1}{2 \left\| \hat{\mathbf{h}}(n) \right\|_1 + \varepsilon}, \quad (18)$$

where ε denotes a small positive constant to avoid division by zero during initialization of the algorithm. The parameter β is a key design parameter because it controls the sparseness of the solution. For example, $\beta = -0.5$ is a typical choice for low sparsity and $\beta = 0.5$ is a typical choice for high sparsity.

When $\beta=-1$, $\mathbf{G}(n)$ becomes a scaled identity matrix and sparse solutions are not promoted anymore. In addition, β may take different values for different subbands since the multipath arrivals are frequency dependent.

b) *The \mathbf{Q} matrix:* The purpose of the \mathbf{Q} matrix is to downweight noise impulses based on their amplitudes. As a consequence, the estimated channel $\hat{\mathbf{h}}$ stays close to the true solution \mathbf{h} under the effect of an impulse. The key assumption here is that the ambient noise, $w_m(n)$, is modeled as complex Gaussian noise, but "contaminated" with impulses (or outliers). It is well recognized that redescending M-estimators can offer protection against complete breakdown in performance due to gross outliers while efficiently treating moderate outliers [15]. Elaborating on the Hampel's three-part redescending M-estimate function [16], the diagonal elements $\{q(e(n-i))\}_{i=0}^{L-1}$ of $\mathbf{Q}(n)$ are given by

$$q(e) = \begin{cases} 1 & , 0 \leq |e|_2 < \xi \\ \frac{\xi}{|e|_2} & , \xi \leq |e|_2 < \Delta \\ \xi \frac{|e|_2 - \Gamma}{\Delta - \Gamma} \frac{1}{|e|_2} & , \Delta < |e|_2 < \Gamma \\ 0 & , \Gamma < |e|_2 \end{cases} \quad (19)$$

The threshold parameters ξ , Δ and Γ are responsible for detecting impulses according to their magnitudes. In addition, these thresholds are adapted continuously so that time-varying second order statistics of the noise are incorporated into the algorithm.

Let $\sigma^2(n)$ stand for the variance of the underlying Rayleigh distribution of $|w_m(n)|$. Using the median operator, a robust recursive estimate $\hat{\sigma}^2(n)$ of $\sigma^2(n)$ is computed as follows:

$$\hat{\sigma}^2(n) = 0.5(\hat{\sigma}_r^2(n) + \hat{\sigma}_i^2(n)), \quad (20)$$

$$\hat{\sigma}_r^2(n) = \lambda_\sigma \hat{\sigma}_r^2(n-1) + c(1-\lambda_\sigma) \text{med}(\text{Re}\{\bar{\mathbf{e}}(n)\}), \quad (21)$$

$$\hat{\sigma}_i^2(n) = \lambda_\sigma \hat{\sigma}_i^2(n-1) + c(1-\lambda_\sigma) \text{med}(\text{Im}\{\bar{\mathbf{e}}(n)\}), \quad (22)$$

$$c = 1.483 \left(1 + \frac{5}{N_w - 1}\right), \quad (23)$$

where $\bar{\mathbf{e}}(n)=[e(n) \dots e(n - N_w + 1)]^\top$ is the observation window of the prior error signal, $\hat{\sigma}_r^2(n)$ and $\hat{\sigma}_i^2(n)$ denote, respectively, the variance of the real and imaginary part of the underlying Gaussian noise, c is a finite sample correction factor and λ_σ is a forgetting factor. $\lambda_\sigma=0.99$ is a typical value. Then, the threshold parameters are chosen by the following expressions:

$$\xi = 2.45\hat{\sigma}(n) \text{ (i.e., } \Pr\{|e|_2 < \xi\} = 0.95), \quad (24)$$

$$\Delta = 2.72\hat{\sigma}(n) \text{ (i.e., } \Pr\{|e|_2 < \Delta\} = 0.975), \quad (25)$$

$$\Gamma = 3.03\hat{\sigma}(n) \text{ (i.e., } \Pr\{|e|_2 < \Gamma\} = 0.99). \quad (26)$$

Note that $O(N_w \log_2(N_w))$ operations are required for the computation of $\hat{\sigma}^2(n)$. Furthermore, $\bar{\mathbf{e}}(n)$ always contains signal-dependent noise from channel estimation errors and thus, the parameter N_w should be chosen close to the channel coherence time.

3) *Decision feedback equalization:* Let L_c and L_a denote, respectively, the causal and acausal taps of the feedforward equalizer and let

$$\mathbf{y}_m(n) = \begin{bmatrix} y_m(nT - (L_c + 1)T/2) \\ \vdots \\ y_m(nT) \\ \vdots \\ y_m(nT + L_a T/2) \end{bmatrix} \quad (27)$$

be the vector of received samples that corresponds to the n^{th} symbol interval. The following expression holds:

$$\mathbf{y}_m(n) = \mathbf{H}_m(n)^\dagger \bar{\mathbf{u}}(n) + \mathbf{w}_m(n), \quad (28)$$

where

$$\bar{\mathbf{u}}(n) = \begin{bmatrix} u(nT - (N_c + L_c - 2)T/2) \\ \vdots \\ u(nT) \\ \vdots \\ u(nT + (N_a + L_a)T/2) \end{bmatrix}, \quad (29)$$

$\mathbf{w}_m(n)$ is the noise vector and $\mathbf{H}_m(n)$ is the channel matrix with the j -th column composed of $\mathbf{h}_m(n - L_c + j)$. Before any detection, the causal ISI from $\mathbf{y}_m(n)$ is removed by using the previous robust channel estimates and symbol decisions. To this end, $\mathbf{H}_m(n)$ is partitioned into causal and acausal parts, namely, $\mathbf{H}_m(n)^\dagger = [\mathbf{H}_c(n)^\dagger \mathbf{H}_{ac}(n)^\dagger]$, where $\mathbf{H}_c(n)$ includes the rows of $\mathbf{H}_m(n)$ that correspond to the causal input signal $\bar{\mathbf{u}}_c(n)=[u(nT - (N_c + L_c - 2)T/2) \dots u((n-1)T)]^\top$ and $\mathbf{H}_{ac}(n)$ includes the rows of $\mathbf{H}_m(n)$ that correspond to the acausal input signal $\bar{\mathbf{u}}_{ac}(n)=[u(nT - T/2) \dots u(nT + (N_a + L_a)T/2)]^\top$. The ISI-free signal at the input of the feedforward equalizer is constructed as:

$$\bar{\mathbf{y}}_m(n) = \mathbf{y}_m(n) - \hat{\mathbf{H}}_c(n)^\dagger \bar{\mathbf{u}}_c(n). \quad (30)$$

The soft estimate of the transmitted symbol d_n is obtained by adding the outputs of all feedforward equalizers, i.e.,

$$\hat{d}_n = \sum_{m=1}^M p_{n,m} \quad (31)$$

$$p_{n,m} = \mathbf{x}_m^\dagger(n) \bar{\mathbf{y}}_m(n) \quad (32)$$

where $\mathbf{x}_m(n)$ is the impulse response of the feedforward equalizer during the n^{th} symbol interval.

Since all subbands carry the same symbols, the filters $\mathbf{x}_m(n)$ can be updated either jointly or in parallel based on minimizing the mean square of the error signal $\varepsilon(n) = \hat{d}_n - d_n$. A recursive approach with fast adaptation to channel fluctuations is based on the RLS algorithm [4]. For joint adaptation, the input vector of the RLS algorithm is $[\bar{\mathbf{y}}_1(n)^\top \dots \bar{\mathbf{y}}_M(n)^\top]^\top$ and so the computational complexity becomes $O((ML_c + ML_a)^2)$. For the remainder of this paper, we call this receiver as R1. For parallel adaptation, the RLS algorithm is invoked M times for each input $\bar{\mathbf{y}}_m(n)$ and so the computational complexity becomes $O(M(L_c + L_a)^2)$. We call this receiver as R2. Since

joint optimization is always better than parallel optimization, R2 performance is always upper bounded by R1 performance provided that the employed RLS algorithm is numerically robust [17].

Note that robustification of the DFE receiver is achieved via the channel estimator. If a strong impulse occurs at time n , it means that the prior error signal $e_m(n)$ is larger than Γ with high probability. In such and only event, the receiver performs two modifications: $I_{n+1,m}=I_{n,m}$ and $\mathbf{x}_m(n+1)=\mathbf{x}_m(n)$. This robustification strategy is sufficient to deal with a small fraction of impulses in the data.

D. Pre-combiner

Further reduction of the computational complexity is possible by pre-combining the M subbands into a smaller number, K , before any Doppler compensation. The pre-combiner is an $M \times K$ matrix of weights, which are adaptively configured through minimizing the common error signal $\varepsilon(n)$. The novelty here with respect to [8] is that different subbands rather than different spatial channels are pre-combined in a way such that frequency diversity is not heavily compromised. In addition, adaptive resampling rather than (narrowband) carrier-phase compensation is performed after the pre-combiner.

The pre-combiner receiver structure is shown in Fig. 2. Let $\mathbf{C}(n)$ denote the pre-combiner matrix, the output of the pre-combiner (sampled at 4 samples/symbol) is given by

$$\sum_{m=1}^M c_{k,m}^*(n) r_m(n'), k = 1 \dots K. \quad (33)$$

The weights $c_{k,m}$ are adapted based on the MSE of $\varepsilon(n)$. Since the number of weights is relatively small (MK), the pre-combiner weights are determined recursively via the RLS algorithm. The RLS update equation is

$$\mathbf{c}(n) = \mathbf{c}(n-1) + \text{RLS}(\varepsilon(n), \mathbf{s}(n)) \quad (34)$$

$$\mathbf{V}(n) = \begin{bmatrix} r_1(nT - (L_c+1)\frac{T}{2}) \dots r_1(nT - L_a\frac{T}{2}) \\ \vdots \\ r_M(nT - (L_c+1)\frac{T}{2}) \dots r_M(nT - L_a\frac{T}{2}) \end{bmatrix} \quad (35)$$

$$\mathbf{s}(n) = \begin{bmatrix} \mathbf{V}(n) \mathbf{x}_1^*(n) e^{-j\phi_{n,1}} \\ \vdots \\ \mathbf{V}(n) \mathbf{x}_K^*(n) e^{-j\phi_{n,K}} \end{bmatrix}, \quad (36)$$

where \mathbf{c} is the column vectorization of matrix \mathbf{C} , \mathbf{V} is the $M \times (L_c + L_a)$ data matrix (sampled at 2 samples/symbol) and $\mathbf{s}(n)$ is the $MK \times 1$ input vector. Initialization of the algorithm starts as follows: at the beginning of the adaptation the entries of \mathbf{C} are kept fixed to zero except for $c_{k,m}=1$, $m=k$, $k=1 \dots K$ for a pre-determined period of $3(L_c + L_a)$ symbol intervals. At the end of the pre-determined period, the equalizers have converged to some meaningful solutions and the pre-combiner starts its adaptation. Similarly to R1, when the K feedforward filters are jointly adapted, we call this receiver as R3. Alternatively, when the K feedforward filters are adapted in parallel, we call this receiver as R4.

III. EXPERIMENTAL RESULTS AND DISCUSSION

We now report on the performance of the proposed receivers R1, R2, R3 and R4 by using field data. The experiment took place in the sea of Selat Pauh, Singapore, on October 21st and 23rd, 2013. The projector was deployed off a vessel, submerged about 3 m below the sea surface. The receiver was a horizontal uniformly-spaced linear array, which was deployed off a second vessel and submerged about 3 m below the sea surface. The sea depth along the link varied about 15-20 m and the sound speed profile was isovelocity (1540 m/s). Here, we use data from one sensor of the array. It is important to note that the projector was rigidly attached on a pole structure and as the transmit vessel was propelling the pole was facing rapid motion-induced vibrations.

The transmitted signal used three subbands: 14.4-16.1 kHz (subband A), 16.1-17.8 kHz (subband B) and 17.8-19.5 kHz (subband C). All subbands carried 4-PSK signals at rate of 1000 symbols/s. Hence, the total bit rate of the link was 2 kbps. Several transmissions at different ranges and vessel velocities were repeated. Here, we examine two ranges: 1 km (file 163012) and 3.1 km (file 150606). Before we present the demodulation results, it is instructive to gain insight into the ambient noise and channel characteristics.

Fig. 3(a) clearly shows that the ambient noise series (14.4-19.5 kHz) includes instantaneous (impulse-like) sharp sounds. The source of these impulses is due to snapping shrimp. Studies have shown that the Symmetric alpha-Stable ($S\alpha S$) distribution efficiently models snapping shrimp dominated ambient noise [11], [12]. Fig. 3(b) verifies this result by plotting the $S\alpha S$ fit along with the Gaussian and the empirical fit of the noise samples of Fig. 3(a). In addition, a Kolmogorov-Smirnov goodness-of-fit test is applied at a 1% significance level. The hypothesis that the noise is Gaussian distributed is rejected while the hypothesis that the noise is $S\alpha S$ distributed is accepted.

Fig. 4(a) and (b) show, respectively, the time evolution of the amplitude of the subband responses of the links 163012 and 150606. As expected, the sparseness of the multipath profile is different for each subband. The time-varying Doppler is decoupled from these responses and is illustrated in Fig. 4(c) and (d). Common resampling of each subband (single time-scale factor estimate) was sufficient for demodulating the data. The subband with the highest SNR was used for time-scale factor estimation. The positive Doppler of 163012 indicates that the transmit vessel was propelling towards the receiver at a varying speed of about 1.5-2.5 m/s. The negative Doppler of 150606, on the other hand, indicates that the transmit vessel was propelling away from the receiver at a varying speed of about 1.5-4.5 m/s. These results are generated by using the R1 receiver in training mode, i.e., the post-cursor ISI is estimated and cancelled based on correct symbol decisions. Due to the high SNR, these channel estimates are very reliable since the receiver can achieve error-free communications.

The receiver performance metric is the symbol error probability (SER) as a function of the received SNR. Since the data

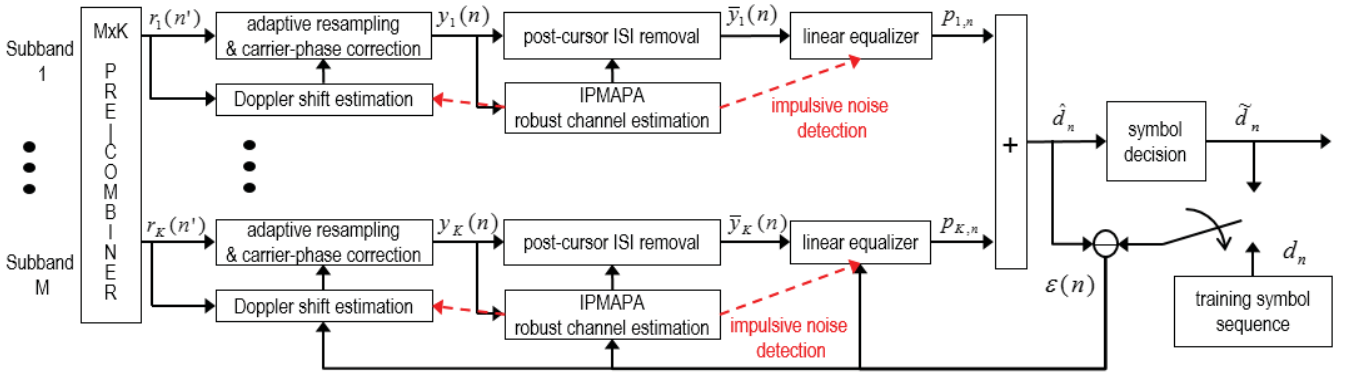


Fig. 2. (a) Block diagram of the MxK pre-combiner receiver.

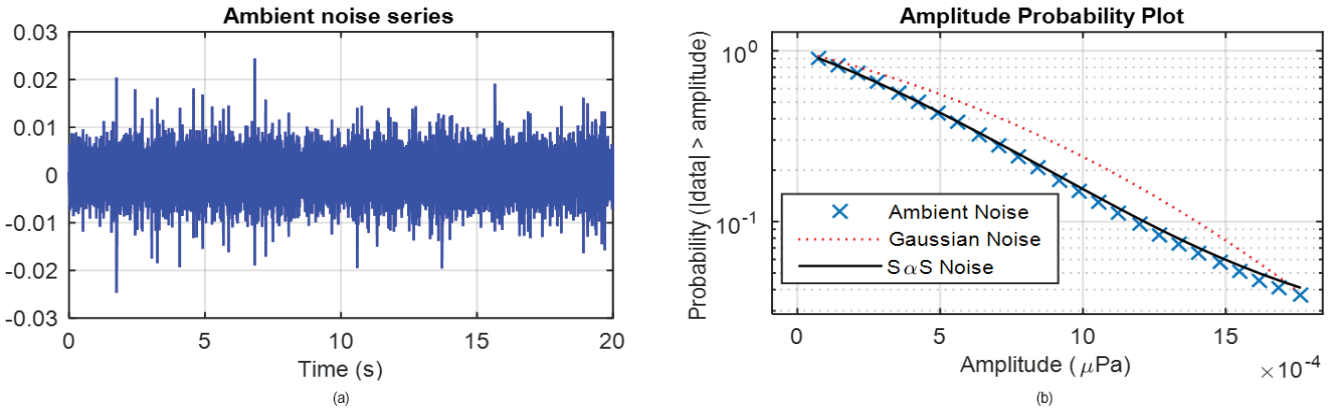


Fig. 3. (a) Recorded ambient noise series. (b) Amplitude probability plots showing that the S α S distribution is a better fit than the Gaussian distribution. S α S fit parameters: $\alpha=1.67$ and $\delta=0.00044$.

was originally acquired in very high SNR, the following plots are computed by scaling and adding extra ambient noise to the original data. At every SNR, the SER is computed after averaging 10 independent ambient noise realizations. Note that the first 900 transmitted symbols were used as a training set for the channel estimator and the RLS equalizer. To ensure a fair comparison between all receivers, the channel estimation parameters μ and N_w are optimized such that the lowest SER is obtained for a given received SNR. The rest of the parameters are shown in Table I.

Fig. 4(e) and (f) show the performance curves for the links 163012 and 150606, respectively. Receivers R3 and R4 use a 3×2 subband pre-combiner each. It is clear that the receiver R1 consistently outperforms all other receivers since it exploits frequency diversity in an optimal manner. The R2 receiver has about 1-1.5 dB power loss with respect to R1 for all SER. The R3 receiver has about 3 dB power loss with respect to R1 for the 163012 channel. Although R4 failed to work in channel 163012 (cannot cope with the time-varying ISI), it managed to demodulate the data for the 150606 channel with a power loss of 1.5 dB with respect to R1. In addition, Table I summarizes the algorithmic complexities as a function of the constituent filter lengths. Note, for example, that R4 require significantly

less computational power than R1.

IV. CONCLUSION

We have presented four low-complexity adaptive DFEs that operate across M parallel subbands. The proposed receivers have successfully managed to: (a) tolerate variable transmitter/receiver mobility (1.5-4.5 m/s) within one signal packet, (b) adapt to rapid multipath fluctuations by exploiting different channel sparseness per subband, and (c) achieve robustness under impulsive noise. The key component of all receivers is the combination of adaptive resampling, sparse robust channel estimation and multichannel equalization.

These receivers require different processing complexities based on how frequency diversity is harvested. Receiver R1 performs joint equalization of all employed subbands while R2 uses M parallel equalizers. Receivers R3 and R4 further decrease the computational complexity of R1 and R2, respectively, by employing an $M \times K$ ($K < M$) subband pre-combiner. The performance-complexity tradeoffs of these receivers have been demonstrated by processing 4-PSK modulated signals from two shallow water links showing excellent results.

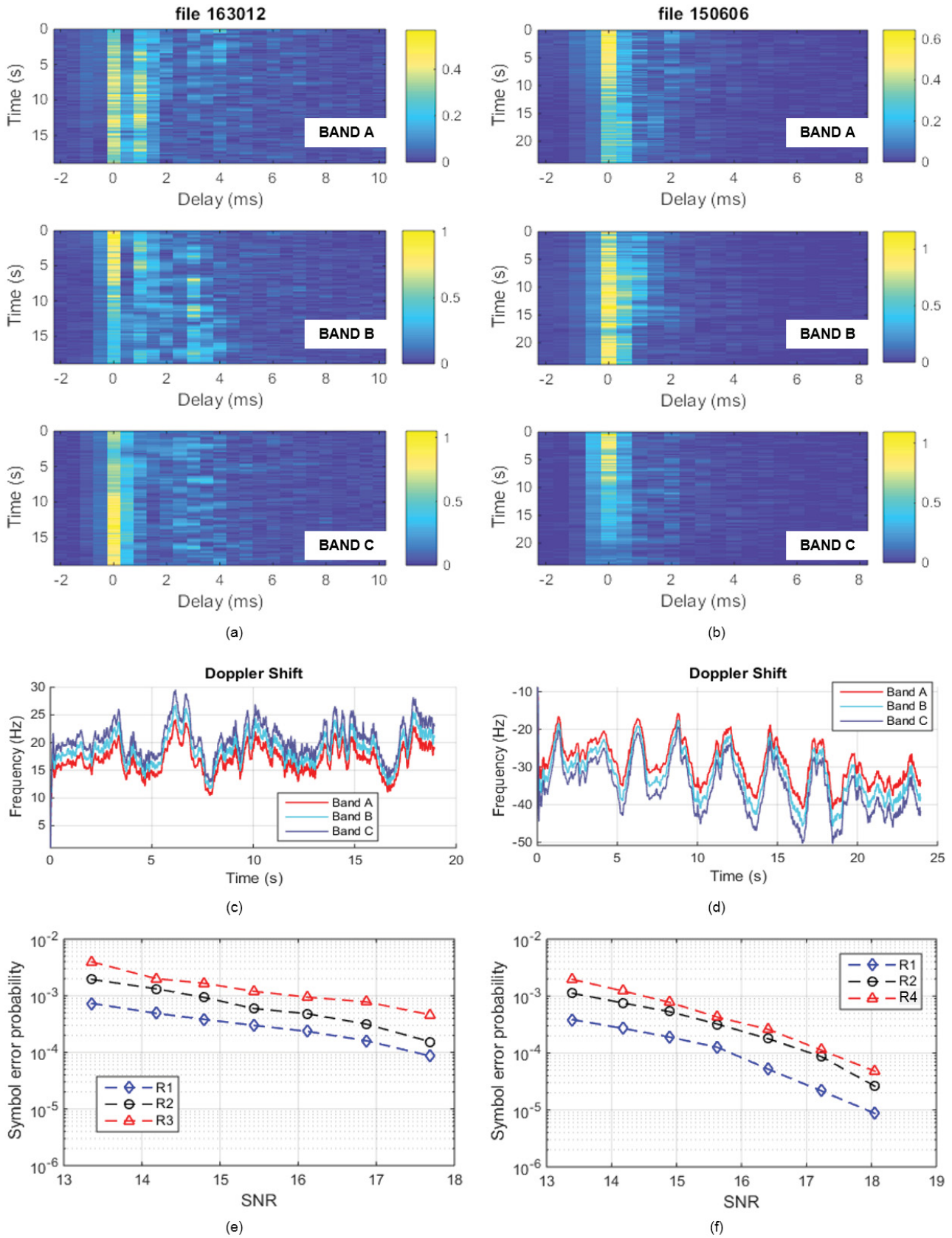


Fig. 4. (a) and (b) show channel impulse responses for channel 163012 and 150606, respectively. For all impulse responses, the x-axis shows multipath delay, the y-axis shows absolute time and the z-axis shows the channel amplitude in linear scale. (c) and (d) show mean Doppler shift vs. time for channel 163012 and 150606, respectively. (e) and (f) show SER vs. SNR for all algorithms for channel 163012 and 150606, respectively.

TABLE I
RECEIVER COMPLEXITIES FOR ALL LINKS

Link 163012 (1 km)			
# of transmitted symbols = 18930 (packet duration=18.9 s)			
receiver	R1	R2	R3
L, β, K_p	1, -0.5, $8 \cdot 10^{-5}$		
$N_c + N_a, L_c + L_a$	25, 9		
IPMAPA complexity	$O(3(N_c + N_a))$	$O(3(N_c + N_a))$	$O(2(N_c + N_a))$
RLS complexity	$O(9(L_c + L_a)^2)$	$O(3(L_c + L_a)^2)$	$O(4(L_c + L_a)^2)$
Link 150606 (3.1 km)			
# of transmitted symbols = 23940 (packet duration=23.1 s)			
receiver	R1	R2	R4
L, β, K_p	1, -0.5, $8 \cdot 10^{-5}$		
$N_c + N_a, L_c + L_a$	21, 9		
IPMAPA complexity	$O(3(N_c + N_a))$	$O(3(N_c + N_a))$	$O(2(N_c + N_a))$
RLS complexity	$O(9(L_c + L_a)^2)$	$O(3(L_c + L_a)^2)$	$O(2(L_c + L_a)^2)$

ACKNOWLEDGMENT

The authors are indebted to Mr. Zou Nan and Mr. Gimhwa Chua of DSO National Laboratories for their leadership during the sea trials in Singapore.

REFERENCES

- [1] M. Stojanovic, J. A. Catipovic, and J. G. Proakis, "Phase-coherent digital communications for underwater acoustic channels," *IEEE J. Oceanic Eng.*, vol. 19, pp. 100-111, 1994.
- [2] J. C. Preisig, "Performance analysis of adaptive equalization for coherent acoustic communications in the time-varying ocean environment," *J. Acoust. Soc. Amer.*, vol. 118, pp. 263-278, 2005.
- [3] M. Stojanovic, J. Catipovic and J. Proakis, "Adaptive Multichannel Combining and Equalization for Underwater Acoustic Communications," *J. Acoust. Soc. Amer.*, vol. 94, no. 3, pp. 1621-1631, 1993.
- [4] S. Haykin, *Adaptive Filter Theory*, 4th ed. Upper Saddle River, NJ: Prentice-Hall, 2002.
- [5] K. Pelekanakis and M. Chitre, "New sparse adaptive algorithms based on the natural gradient and the L_0 -norm," *IEEE J. Ocean. Eng.*, pp. 323-332, vol. 38, 2013.
- [6] K. Pelekanakis and M. Chitre, "Adaptive Sparse Channel Estimation under Symmetric alpha-Stable Noise," *IEEE Trans. on Wireless Communications*, vol.13, no. 6, pp. 3183-3195, 2014.
- [7] M. Stojanovic, J. A. Catipovic, and J. G. Proakis, "Reduced-complexity spatial and temporal processing of underwater acoustic communication signals," *J. Acoust. Soc. Amer.*, vol. 98, no. 2, pp. 961-972, Aug. 1995.
- [8] M. Stojanovic, "Efficient processing of acoustic signals for high rate information transmission over sparse underwater channels," *J. Phys. Commun.*, pp. 146-161, 2008.
- [9] P. A. van Walree and G. Leus, "Robust underwater telemetry with adaptive turbo multiband equalization," *IEEE J. Ocean. Eng.*, vol. 34, no. 4, pp. 645-655, October 2009.
- [10] M. Bouvet and S. C. Schwartz, "Comparison of adaptive and robust receivers for signal detection in ambient underwater noise," *IEEE Trans. Acoust., Speech, Signal Processing*, vol. ASSP-37, pp. 621-626, 1989.
- [11] M. A. Chitre, Underwater Acoustic Communications in Warm Shallow Water Channels, PhD thesis, Department of Electrical and Computer Engineering, National University of Singapore, 2006.
- [12] M. W. Legg, *Non-Gaussian and non-homogeneous Poisson models of snapping shrimp noise*, Ph.D. thesis, Department of Imaging and Applied Physics, Curtin University of Technology, 2010.
- [13] C. P. Shah *et al.*, "Low-Complexity Iterative Receiver Structure for Time-Varying Frequency-Selective Shallow Underwater Acoustic Channels Using BICM-ID: Design and Experimental Results," *IEEE J. Ocean. Eng.*, vol.36, no.3, pp. 406-421, 2011.
- [14] J. Benesty and S.L. Gay, "An improved PNLMS algorithm", in *Proc. IEEE ICASSP*, vol.2, pp. 1881-1884, 2002.
- [15] A. M. Zoubir *et al.*, "Robust Estimation in Signal Processing: A Tutorial-Style Treatment of Fundamental Concepts," *IEEE Signal Processing Magazine*, vol.29, no.4, pp. 61-80, 2012.
- [16] S. C. Chan and Y. Zou, "A Recursive Least M-Estimate Algorithm for Robust Adaptive Filtering in Impulsive Noise: Fast Algorithm and Convergence Performance Analysis", *IEEE Trans. Sig. Processing*, vol. 52, no. 4, pp. 975-991, 2004.
- [17] S.C. Douglas, "Numerically-robust O(N2) RLS algorithms using least-squares prewhitening," in *Proc. IEEE ICASSP '00*, vol. 1, pp. 412-415, 2000